246840-1-F

Final Report
PRISM GROUND EXPERIMENT

B. Neagle
A. Klooster

March 1995

Sponsored by:

ARPA/ASTO
3701 North Fairfax Drive
Arlington, VA 22203-2724

Wright Laboratory/AARI-2
Wright-Patterson AFB, OH 45433-6543

Contract No.: DLA900-88-D-0392
Delivery Order: 38

P.O. Box 134001
Ann Arbor, MI 48113-4001

DISCLAIMER NOTICE

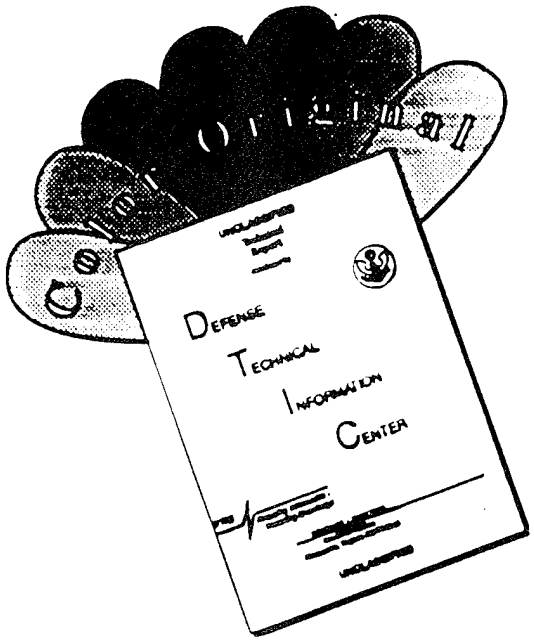

THIS DOCUMENT IS BEST QUALITY AVAILABLE. THE COPY FURNISHED TO DTIC CONTAINED A SIGNIFICANT NUMBER OF COLOR PAGES WHICH DO NOT REPRODUCE LEGIBLY ON BLACK AND WHITE MICROFICHE.

ERIM-320

REPORT DOCUMENTATION PAGE

Form Approved
OMB No. 0704-0188

1. AGENCY USE ONLY (*Leave Blank*)	2. REPORT DATE	3. REPORT TYPE AND DATES COVERED
	March 1995	Final

4. TITLE AND SUBTITLE
PRISM Ground Experiment Final Report

5. FUNDING NUMBERS

6. AUTHOR(S)
B. Neagle and A. Klooster

7. PERFORMING ORGANIZATION NAME(S) AND ADDRESS(ES)
Environmental Research Institute of Michigan
P.O. Box 134001
Ann Arbor, MI 48113-4001

8. PERFORMING ORGANIZATION REPORT NUMBER
246840-1-F

9. SPONSORING/MONITORING AGENCY NAME(S) AND ADDRESS(ES)
ARPA/ASTO
3701 North Fairfax Drive
Arlington, VA 22203-2724

Wright Laboratory/AARI-2
WPAFB, OH 45433-6543

10. SPONSORING/MONITORING AGENCY REPORT NUMBER

11. SUPPLEMENTARY NOTES

12a. DISTRIBUTION/AVAILABILITY STATEMENT
Unlimited

12b. DISTRIBUTION CODE

13. ABSTRACT (*Maximum 200 words*)

The 3-D Imaging performance of the PRISM Demonstration System is reported. Design of the sensor vehicle, and control system is presented. Fabrication and local system testing are described. Field experiments at the Kinzua Bridge test site are described. A complete presentation of all the 1994 PRISM images is given in a data catalog titled MOBILE PRISM DEMO IMAGE DATABASE.

14. SUBJECT TERMS	15. NUMBER OF PAGES
PRISM, 3-D Imaging, Kinzua Bridge	45
	16. PRICE CODE

17. SECURITY CLASSIFICATION OF REPORT	18. SECURITY CLASSIFICATION OF THIS PAGE	19. SECURITY CLASSIFICATION OF ABSTRACT	20. LIMITATION OF ABSTRACT
Unclassified	Unclassified	Unclassified	Unlimited

CONTENTS

FIGURES

TABLES

1.0 INTRODUCTION

This report describes the design, fabrication and testing and experimental imaging results of a ground based infrared PRISM system. This work comprised the ground experiment effort of a larger program called the PRISM Demonstration System Design Program, which included sensor modeling and detection modeling efforts. For a description of the theoretical foundation operations of a PRISM sensor please refer to the sensor modeling final reports [1] and [2].

2.0 SYSTEM DESIGN

2.1 GENERAL DESIGN CONSIDERATIONS

The design of the PRISM mobile sensor was driven by top level specifications which were established by the sensor modeling and detection modeling efforts. These specifications, which are summarized in Table 1, were determined from a variety of considerations. For example, the near-nadir viewing geometry and 10 degree angle diversity limits arise from the need to obtain a clear line-of sight to targets hidden in a forested environment. The resolution specifications, on the other hand, are expectations of what might be required to detect and perhaps recognize such objects in clutter from passive 3-D imagery.

Table 1. PRISM Sensor Specification

Angle-angle resolution $<.5$ meters at 100m range Height resolution $<.5$ meters with <40 angular measurements Angle-angle FOV >20 m at 100 m Height FOV >20 m with $<=10°$ angular diversity 3-D sensitivity: MDTD (edge) $<=0.1$ K
Grating optical quality (random) $<=0.05$ waves rms Grating optical quality (quadratic) $<=0.13$ waves rms Grating tilt misalignment $<=150$ arcsec Grating rotational misalignment 30.0 arcsec Grating frequency mismatch <0.005 lp/mm Lateral grating vibration <0.50 microns rms

The sensitivity specification is based on prior estimates of high spatial frequency target and background contrast. Because of the bandpass nature of the sensor, its ability to range is dependent not only on scene contrast, but also subpixel spatial structure. The NETD specification provides a metric for contrast and spatial structure based on a target of known spatial structure - an edge aligned orthogonally to the sensor shear direction. This metric was determined through prior high resolution IR image measurements of a limited set of targets and backgrounds. Most of these measurements showed higher contrast in the 10-20 cycles/m spatial frequency range than a 0.1 C edge; therefore,a sensor designed to provide an accurate range to a 0.1 C edge would also be expected to range to such targets and backgrounds in most environments.

In addition to these top level specifications, two other issues formed the basis of the sensor design. The first of these was the decision to implement a ground based demonstration from the Kinzua viaduct site. This set the operating range to approximately 90 m. The second was the decision to utilize an off-the-shelf Cincinnati Electronics IRC-160 InSb camera as the thermal imaging sensor.

The Kinzua viaduct site was the obvious choice for operation of the PRISM demo sensor. The site has been used by ERIM personnel in the past for testing of prototype sensors. This familiarity greatly simplifies experiment planning. The viaduct was built for coal train traffic in the early part of the 20th century. Current activity on the viaduct is minimal, with excursion train traffic only on weekends in the fall of each year, making experiment logistics manageable. The height of the viaduct, which is approximately 300 feet at the center allows for a nearly downlooking geometry with a reasonable field of view on the ground below. The train track crossing the viaduct makes a very stable, straight and level guide for the traverse of the sensor. The undeveloped natural terrain also makes a good background for camouflaging target vehicles in a realistic setting.

The choice of the Cincinnati Electronics IRC-160 camera was driven largely by cost. The experiment budget allowed for approximately $30K for a thermal imaging focal plane array based camera system. This was to include the appropriate lenses, and

electronics to interface the camera to a computer system. To achieve the field of view and resolution goals, the array needed at least 60 x 60 elements. These requirements quickly narrowed the possible array technologies to only indium antimonide (InSb), and camera vendors to Cincinnati Electronics and Amber Engineering, both of which manufacture their own arrays. The Cincinnati Electronic IRC-160 (described in Table 2) was the one camera that fell within the budget of the project. A unit from Amber which used a 256 x 256 element InSb array was approximately $15 K more. Given the resolution goals and the field of view limits imposed by the PRISM interferometer, the larger AMBER array would be pointless.

Table 2. CE IRC-160 Camera Specification

Array Format	160 x 120 elements
Detector Type	InSb photo diode
Operable Yield	>99%
Spectral Range	1 to 5.5 micron
Quantum Efficiency	70%
Pixel Size	28 micron square on 50 micron square
Operating Temperature Range	30 K to 80 K
Focal Plane D-Star	1×10^{11} Hz cm/watt
Multiplexer Type	CMOS switch array
Input Circuit	Direct Injection
Integration Capacity (full well)	3×10^{7} electrons
Number of Outputs	1
Readout Noise Floor	1000 electrons
Maximum Readout Rate	2 MHz
Stare or Integration Time	Controllable from 1.67% of frame to full frame
Multiplexer Responsivity	6.7×10^{-8} volts/electron
Bias Supplies	6
Pixel Addressing	Sequential Access
Power Dissipation	<10 milliwatt

2.2 OPTICAL SENSOR

The operational wavelength of the system was limited by the camera to the 3 to 5 μm atmospheric window. However, to achieve the desired field of view (FOV), the optical bandwidth of the camera must be further limited by a cold filter.

The critical component of the sensor design is that of the interferometer. In general, it is preferred to utilize a reflective grating interferometer arrangement [Figure 1(a)] since this maximizes sensor throughput and minimizes interferometric (higher orders) and non-interferometric (stray light and component radiation) spurious signals. Because of the near range relative to the desired FOV, however, such a design was not feasible for the ground demonstration sensor since the shear distance (roughly 5-10 mm for 0.2-0.5 m range resolution with 10 degree angle diversity) is less than the aperture size (11 mm). Instead, a transmissive grating interferometer design [Figure 1(b)] was utilized based on square wave phase grating designed to optimize $\pm$ 1 diffracted order efficiency.

The selection of grating periodicity is another critical design issue. On one hand, the periodicity must be sufficient to place singly diffracted scene energy off the detector array. This requirement is satisfied if the grating diffraction angle is greater than the sensor lateral FOV. On the other hand, increasing the diffraction angle decreases the achromatic FOV. The grating parameters given in Table 3 below allow a 13.6 degree FOV with adequate achromatic bandwidth.

Table 3. ZnSe Lamenar Transmission Gratings

Substrate Specifications

Material:	Zinc Selenide, chemical vapor deposited
Refractive Index:	2.43 at 4.7 microns
Diameter:	2.00 $\pm$ 0.01 inches
Thickness:	0.20 $\pm$ 0.01 inches
Clear Aperture:	90% central diameter
Flatness:	less than $\lambda/2$ peak irregularity at 633 nm measured in transmission
Parallelism:	less than 3 arc minute
Surface Quality:	20 - 10 scratch-dig
Coating:	single layer AR coating on one side (unruled) for $<$ 0.5% reflectance at 4.7 microns

Ruling Specifications

Ruled Area:	1.25 inches x 1.25 inches (center of substrate)
Grating Type:	square wave phase (Lamenar)
Duty Cycle:	50 $\pm$ 1%
Periodicity:	50.000 $\pm$ 0.005 1p/mm (relative)
Ruled Depth:	1.64 $\pm$ 0.20 microns

The higher order diffraction effects of the sensor grating are minimized by using a simple baffle system to limit the input FOV. A 4 inch wide aperture 11 inches in front of the grating pair fully admits the 13.6 degree FOV. The walls of the chamber between the aperture and the gratings are painted black to provide a uniformly radiant surface for the higher order diffraction components of the camera image.

Grating alignment is critical for proper operation of the interferometer. Angular alignment tolerances were chosen on the basis of 98% modulation depth. Allowable reltive tilt between the gratings is 2.6 arc min. In-plane rotation of one grating with

respect to the other grating is limited to 37.5 arc sec. The grating phasing (lateral motion of one grating relative to the other) must be precise to 0.5 microns (18 degrees relative phase).

Grating Mount Design

To achieve the high degree of precision specified by the tolerances given above, a rigid/flexure box structure was used as the basis for the interferometer grating translation mount. Details of the design are shown in Figure 2. The flexure box is composed of two identical machined aluminum channel members adhesively bonded to form an open ended box with rigid front and back plates and flexible sides. The rigid plates are bored to accept the two circular gratings in flanged mounts. One grating is held stationary by a right angle bracket that is bolted directly to the sensor baseplate. The second grating is translated on its flexure mount responding to the extension of a piezoelectric pusher. The barrel of the pusher is directly clamped to the stationary grating mount so that positive motion of the moving grating relative to the fixed grating is assured.

Four discreet grating positions representing 0, 90, 180, and 270 degree phasings of the interferometer are used during the data collection. The relative motion of the moving grating to produce these phase shifts are 0, 2.5, 5.0, and 7.5 microns. These grating moves are produced by a Burleigh model PZL-030 low voltage piezoelectric pusher driven by a Burleigh model PZ-150M amplifier. Drive voltage calibration was determined by measuring the motion of the moveable grating with a Brown & Sharpe model 964 electronic gauge. Hysteresis effects in the piezoelectric drive were accommodated by using a repeating stair step move sequence.

The camera, gratings and baffle were mounted on a 2′ x 2′ Newport optical breadboard as shown in Figure 3. The optical axis of the sensor was turned 90 degrees down by means of a right angle mirror supported by the baffle structure. This arrangement allowed the camera to operate in a nominally upright orientation as dictated by the camera dewar filling requirements.

2.3 VEHICLE AND POINTING CONTROL SYSTEM

Pointing Geometry

System pointing geometry is shown in Figure 4. The sensor looks down at the natural terrain below at a distance of about 300 feet and a depression angle of approximately 70 degrees. Data is collected at equally spaced sensor locations along the bridge rail between points A and B. At the center of the traverse (point C) the range to the primary aim point P is a minimum. As the sensor moves from A to B the line-of-sight is maintained in alignment with point P and the sensor rotates around the line P-P" which is perpendicular to the Plane ABP. Point S is a secondary aiming point used by the pointing control system as explained later.

Pointing Error Limits

The allowable along track (pitch) angular error limit is related to the equivalent phase error as determined by the virtual angular fringe spacing. For 50 lp/mm gratings spaced at 12.5 mm the angular fringe spacing is 0.8 mrad and 1/10 wave error limit corresponds to 80 microradians p-p. The IR camera has a 50 micron array spacing and a 25 mm focal length lens yielding a 2 mrad sampling interval. The allowable cross track angular error limit is 1/10 of the angular sampling interval at the camera or 200 microradians p-p. The allowable sensor rotation around the line-of-sight is again related to the virtual fringe error at the top and bottom of the image field. At a 100 meter range and a point 20 meter above or below the aim point the maximum lateral position error is 8 mm. The corresponding rotation angle equal to $.008/20 = 4 \times 10^{-4}$ rad = 400 microradians p-p.

Sensor Travel and Speed Requirements

The maximum sensor vehicle travel distance, dictated by the required 10 degree angular collection interval, is approximately 55 feet. Data were collected at as many as 81 positions requiring 80 moves for a full data collection run. The maximum position error limit based on 1/10 wave error at edge of the field-of-view is 4.4 inches. A maximum data collection time goal of 20 minutes was chosen to minimize the effects of

scene temperature drifts during the data collection.

Sensor Vehicle and Pointing Design Concept

Design of the sensor vehicle was strongly influenced by the physical characteristics of the Kinzua bridge track and pedestrian walkway. To accommodate the 70 degree line-of-sight depression angle it was necessary for the sensor to be located very near the bridge rail so that is could look over the rail and down at the terrain below. It was also recognized that the sensor platform must be stabilized and isolated from vibrations of the bridge walkway produced by pedestrian traffic and wind effects. A design utilizing a dolly riding on an auxiliary track laid next to the bridge rail was pursued. In the final design, one rail of the existing railroad track was also utilized.

The sensor pointing system was designed to track a pair of optical retroreflectors to produce an effective rotation of the sensor platform around an axis fixed to target coordinates. A HeNe laser provided the illumination for the reflectors. The sensor line-of-sight was locked to the primary retroreflector by the tracking system. A secondary retroreflector was used to control sensor rotation around the line-of-sight.

Vehicle Design

The sensor vehicle rides along one existing rail and one auxiliary rail on the bridge deck. Figure 5 shows an along track view of the vehicle and its working position on the bridge. Additional wheels spaced at standard railroad gauge allow easy transportation of the vehicle to and from the data collection area using the existing track.

For the auxiliary rail, American Standard 3 x 5 inch I beam sections in 8 foot lengths are bolted together to create a 64 foot track length. The 8 foot length was chosen to match the spacing of the main cross ties on the bridge deck. The track joints are located directly over the cross ties for maximum stability.

The vehicle is driven along the track by a high torque (600 oz in) stepping motor coupled to a rigid drive axle using a chain drive. The drive wheels are flanged and slightly tapered for self centering action. The stepper motor is controlled by the signals from the Compumotor indexer installed in the PC. When the drive acceleration and

deceleration values were optimally set, move time intervals of less than 5 seconds per move were possible. Overall position accuracy was better than 1 inch.

Sensor Pedestal

The sensor pedestal supports the sensor table kinematically and provides three axis angular control for sensor pointing. A modified version of the pedestal used for the PRAISE data collection [3] was employed. A new lightweight support column was fabricated from 3/8" aluminum plate. The configuration of the pedestal is shown in Figure 6. A tilt plate mounted on a single central ball joint provides for two degrees of angular motion of the sensor platform. Servo motor driven linear slides drive the tilt plate around two orthogonal axes. A flex plate with a ball joint end mounted on one slide drives the pitch axis. A double ball joint link controls the roll axis. The central ball provides three positional constraints at the center of the tilt. The flex plate with a ball joint supply two additional constraints. The flex link supplies the sixth constraint to kinematically locate the tilt plate with respect to the support column.

A motor driven rotary stage mounted on the tilt plate rotates the sensor platforms around the yaw (vertical) axis. The sensor line of sight is designed to lie parallel to this axis.

Pointing Control System

The pointing control system is a closed loop servo system used to control the three motorized stages of the pedestal. The pitch and roll drives align the sensor line-of-sight to a retroreflector located at scene center as depicted as point "P" in Figure 4. The yaw (rotary stage) channel is locked to a secondary retroreflector outside of the sensor field-of-view.

The control components of the sensor system are identified in the system block diagram, Figure 7. The retroreflector illumination and detection components are located on the sensor table. The pointing control drives the pedestal to close the pointing loop.

The sensor table components of the pointing control system are shown in Figure 3. A 9X rifle scope mounted on the table provided a view of the target field. The HeNe

laser projects a pair of beams directed toward the retroreflectors. Each beam spreads to about one foot diameter at 300 feet. The returned beams are collected by a 16 inch focal length lens and focussed to a pair of lateral effect photodetectors mounted on a linear translation stage. The primary beam and secondary beams are monitored by dual axis and single axis detectors respectively. A United Detector Technology Model 431 X-Y Position Indicator generates spot position error signals for the primary beam's dual axis detector. The X position error is amplified and drives the roll axis of the pedestal to close the roll pointing servo loop. The Y position error drives the pedestal pitch axis. The secondary beam detector output is sensed by a UDT Model 301 DIV conditioning amplifier. The amplifier output, representing sensor yaw error, is amplified and used to drive the pedestal rotary stage.

Incremental translation of the linear stage during data collection allows the effective location of the primary retroreflector to be moved upward or downward. The translation stage motion is computer controlled and the effective offset distance is entered as a data collection parameter in the system control program.

Operating modes of the pointing control are selected by switches on the control panel. Separate switches for the primary and secondary control loops are provided. A manual operating mode utilizing a joystick controller allows the sensor to be driven to the point where the outgoing laser beams illuminate the retroreflectors. Generally, the primary retroreflector is acquired first by a manual search of the target area as seen through the rifle scope. When the returned laser beam is detected, the primary loop is automatically closed and automatic tracking of the primary retroreflector is maintained unless the returned energy falls below a manually set threshold. The yaw axis is manually rotated to search for the secondary retroreflector. Detection is evidenced by a jump in signal power output from the secondary detector amplifier. The secondary channel then automatically switches to track mode. The three axes of the pedestal are thus locked to the pointing references and are able to maintain lock as the sensor vehicle moves along the track.

System pointing errors were monitored by using an oscilloscope to observe the voltage outputs from the X-Y position indicator. Using the scaling factor of 2.84 mv/microradian, a voltage swing of 227 mv corresponds to a 1/10 wave error limit for the X (pitch) channel. During field operations, voltage swings exceeded 100 mv only during extremely strong wind gusts.

2.4 DATA ACQUISITION AND SYSTEM AUTOMATION

The PRISM sensor system includes several subsystems which must be controlled (by digital computer) in a well defined sequence to collect thermal imagery that can be successfully processed into three-dimensional images. These functions include: lateral grating motion, IR camera signal digitization and a data storage, sensor position, and sensor pointing system offset. Figure 7 shows a block diagram of the PRISM system. All data acquisition and automation is controlled by a PC compatible computer through a series of ISA bus analog and digital interfaces. Lateral grating motion is achieved by generating an analog voltage using a Metrabyte A/C converter card. The voltage signal is amplified and used to drive a piezo-electric positioner which moves the grating to the four desired positions. Due to hysteresis in the positioner, care was taken to always step the grating to a desired position from the same direction.

The PC also contains a step motor indexer card (Compumotor PC-23) which is programmed to generate step and direction pulses for steps motors controlling sensor along-track positioning and pointing system detector offset.

IR camera data acquisition is accomplished with a digital interface supplied with the Cincinnati Electronics IRC-160 camera. This interface includes memory for storage of 27 frames which can be collected in sequence. Data from these buffers is transferred to the PC using direct memory access.

A system control program was written for the PC which sequenced each of the devices described above through a data collection. At run time, the software reads a control file which includes collection parameters pre-defined by the operator. A flow

diagram of the code as it was used int he 1993 data collection is shown in Figure 8. Simulations run during the system design had determined that 50 frames of each phase should be collected and averaged to get the desired signals to noise ratio. Because of the limited memory and lack of accumulation hardware on the camera acquisition board, it was necessary to acquire this in two groups of 25 frames which were accumulated (averaged) in the PC. In this collection scheme, the 4 phases were collected in order 0 through 270 degrees, with a full sensor position collected in just under 1 minute.

While analyzing data from the 1993 collections, artifacts due to scene bais were found. As described above, the time between collection of 180 degree phase shifted images (i.e. 90 and 270) had been nearly 20 seconds. These pairs of frames were subtracted to remove signals bias, but small changes in scene temperature over this 20 seconds results in imperfect bias cancellation.

To solve the problem, a new acquisition sequence was devised and is shown in Figure 9. To implement this new sequence quickly, two hardware upgrades were necessary. The first was the addition of a larger memory buffer for the camera acquisition board. The new buffer was large enough to hold over 100 sequential frames from the camera. This allowed all frames forming a pair of phases to be collected without interruption. As shown in the flow diagram, these frames were collected in an interleaved fashion so that any low order bias changes will cancel.

The second upgrade was a faster PC to speed the frame averaging, further decreasing the total collection time to minimize possible bias fluctuations. This scheme was successfully used for all of the 1994 data collections.

3.0 SYSTEM FABRICATION AND TEST

3.1 PEDESTAL AND POINTING SYSTEM

The pedestal and pointing sub-system was assembled and tested using the facilities of ERIM's Compact Test Range. The pedestal base was bolted to 4′ x 8′ optical table and the optical components of the pointing system were mounted on the 2′ x 2′ sensor

baseplate. Closed loop operation of the pointing system was tested by setting up a pair of retroreflectors at a 100 meter range. The downward looking characteristic of the pointing sensor was accommodated by mounting a large turning mirror below the sensor on the optical table. Loop gains were adjusted for maximum sensitivity without oscillation. Control loop error signals were monitored to determine pointing accuracy. The test results are listed below:

Pitch error signals:	14.2 microradians p-p (limit 80 rms)
Roll error signal:	11.4 microradians p-p (limit 200 rms)
Yaw error signal:	32.6 microradians p-p (limit 400 rms)

Note that the measurements represent peak-to-peak errors. RMS values would be substantially lower.

3.2 SENSOR ASSEMBLY AND TESTING

The grating interferometer elements of the PRISM sensor were aligned by observing the diffracted orders produced by the grating pair when illuminated by a HeNe laser source. The laser beam was expanded and collimated before illuminating the grating pair. The interference patterns produced by the diffracted orders were observed and the rotation of one grating relative to the other was adjusted until vertical fringes were observed in the interference patterns. This procedure allowed the rotation to be aligned to the required 30 arc-second tolerance. The 3 arc-minute parallelism tolerance was assured by the mechanical tolerances of the mounting structure.

The IR camera and interferometer were bolted to the sensor baseplate and the IR sensor optical axis aligned to that of the pointing system. A thermal line source was set up at a distance of 100 meters and imaged by the camera. Image intensity modulation levels were measured as a function of grating shift. The interferometer was capable of producing the required modulation levels.

3.3 VEHICLE FABRICATION AND TESTING

Preliminary test of the sensor vehicle were made using a 16 foot track setup in the assembly building. The stepping motor drive was shown to have adequate torque to make the required vehicle move steps in less than 5 seconds.

3.4 LOCAL RANGE SYSTEM TRIALS

Full system operational capability was verified by full scale testing on a horizontal range. A 64 foot operating track was set up on ERIM property using the I beam rail sections fabricated for use at the Kinzua site. Vehicle move accuracy was verified for a full move sequence. Accumulated move errors never exceeded 1/2 inch for a full data collection sequence.

Horizontal operation of the sensor was accomplished by removing the turning mirror assembly and reconfiguring the pointing system axis assignments. The primary retroreflector was set up at a range of 100 meters on a line perpendicular to the center point of the track. A temperature controlled edge target and line target were set up near the center of the sensor FOV but at a nearer range to simulate the field exercise geometry. Full sensor data runs were recorded and processed to verify system performance. Figure 10 shows the PRISM System range impulse response for an offset line target.

4.0 FIELD EXPERIMENTS

The sensor system and supporting equipment was transported to the Kinzua Viaduct test site for field exercises on five occasions; three times in the Fall of 1993 and twice in the Summer of 1994. The objective of these exercises was to collect data representing natural terrain, military vehicles, and calibrated test targets. The 2000 foot length of the bridge allowed the selection of several imaging scenes (each roughly 80' x 80') with distinctly different properties. The experiments utilized three of these scenes. The first

scene included terrain with an abrupt drop, many visible large rocks and a dirt path for placement of target vehicles. The second scene contained a sloping terrain with heavy vegetation cover. Targets in this scene were parked on a small overgrown path with overhanging trees. The final scene was relatively flat with a few tall trees and ground foliage that had been cut to a height of less than 6 inches. The range to the centers of each scene were between 280 and 315 feet with nadir angles between 15 and 25 degrees. A total of 25 images were collected at these three sites during the Fall collections in 1993. An additional 85 images were collected using the upgraded sensor system in 1994.

The initial field operations were highly successful. The overall system concept was demonstrated and no significant system failures were encountered. The September 1993 data was generally of good quality except for the data runs taken when the average scene temperature was changing over the collection time. The image artifacts occurring under these conditions were attributed to the 20 second time interval between data collected for the zero and pi phase shift conditions of the grating interferometer. These drifts made it impossible to properly subtract the scene bias from the interferometer signals. The data were also collected in complex format with processed ranges extending equally above and below the aiming point. The lack of DC response in the image formation produced a blank stripe through the zero range plane of the image. This would be eliminated for the 1994 collection by shifting the DC plane using an offset aiming point.

An example of the imagery generated from the 1993 data is shown in Figure 11. The two upper images are grey scale encoded range maps of an open and netted M35 truck. The lower images are along track projections of the 3D images showing the blank stripe centered on the zero range plane.

The PRISM demonstration system was upgraded for the 1994 data collections. New hardware was installed allowing the zero and pi phase shift to be recorded contemporaneously. An offset aiming feature was also included allowing the DC artifact to be removed from the zero range position in the output images. A total of 85 data runs were made using the upgraded sensor system. Precise ground truth data for the two

scene locations used were recorded for subsequent comparison with the processed imagery. The image artifacts noted in the 1993 data were essentially eliminated and the 3-D imaging potential of the PRISM sensor system was amply demonstrated

5.0 DATA COLLECTION RESULTS

5.1 3-D IMAGE FORMATION

Field data files from the 1994 collections were transferred to the ERIM Optical Science Lab computer systems for subsequent 3-D image formation processing. These data files contained the averaged image data described in section 2.4 and the computed range and look angle for each image. The image data were computer processed using PRISM image formation software. The processor output was in the form of a 1D Fourier transform of pixel intensity fluctuations vs. sensor look angle for each x, y image pixel. A pixel walk algorithm was employed to account for perspective changes in the images image data. The resulting 3-D data was converted to a 3-D surface (2D array) by choosing an estimated unique range for each pixel. Range estimates were chosen as the location of the strongest peak in the transform. No estimate was made if the peak did not exceed a user defined threshold.

The 3-D surface generating capability of the PRISM sensor is illustrated in the 3-D surface plot for run #1 shown as Figure 12 where the height of the camouflage net, target vehicle (HMMWV), and trees is shown with respect to a well defined ground plane. The change detection capability of the sensor is illustrated in Figure 13 where the surface data from run #5 was subtracted from that of run #1. Here the target vehicle which was moved under the camouflage net for run #5 is shown clearly as a positive value surface on a zero value background.

A complete presentation of all the PRISM image data is given in a data catalog [4] titled MOBILE PRISM DEMO IMAGE DATABASE. Entries in the database include a cover page listing the target description and scene photograph if available, a second page showing a reference thermal image and a PRISM signal strength image, and a third

page presenting the PRISM scene in the form of a color encoded range map. A log describing the 85 data collection runs is included in the section as Table 4. No PRISM images were generated for data runs listed with data type "No Grating". For these runs, the gratings were removed from the sensor to allow reference images to be recorded for image quality control.

5.2 RANGING ACCURACY MEASUREMENTS

A detailed survey of the ground features at PRISM Site #1 was performed during the June '94 field exercise. A precision theodolite with electronic distance measurement (EDM) was used to catalog the location of the ground surface at 65 randomly selected positions in the sensor field of view. The along track, cross track, and height coordinates of the surveyed points relative to a horizontal plane passing through the primary retroreflector were calculated from the survey data. These coordinates were transformed to a coordinate system based on the sensor viewing geometry so that the z axis measurements would represent height in sensor coordinates. The PRISM range data from run #1 of 6/20/94 was compared point by point to the survey data. The predicted minus actual range for each survey point was tabulated and an error histogram generated using a bin size of 0.2 meters. The resulting distribution shown in Figure 14 (a) shows a very strong grouping of errors around the zero error bin which has the highest number of occurrences. The five error values greater than 2 meters are likely to be anomalies and were removed to give the more representative distribution shown as Figure 14 (b). The mean error for this set of measurements was 0.05 meter which indicates the absence of any systematic bias in the measurement process. The standard deviation of the errors was 0.43 meters and probable error is 0.29 meters assuming a normal distribution. These results are quite remarkable given that the measured PRISM range IPR 3 dB width was 0.48 meters

Given the high level of ranging accuracy demonstrated by the PRISM system using the first image data set, no further verification tests were performed.

6.0 CONCLUSIONS

For the first time ever, we have demonstrated the ability to perform passive 3-D interferometric imaging in the infrared spectral region of full-sized targets in a natural clutter environment. Test target results have validated the theoretical foundations and a detailed sensor performance model, and 3-D image results have indicated that a measurable target and background signature exists even at night. The accuracy of the ranging capability was determined by detailed comparison with accurate ground truth survey data and a change detection capability was demonstrated.

7.0 REFERENCES

[1] M.T. Eismann, *PRISM Sensor Modeling*, ERIM Final Report No. 246850-1-F, Environmental Research Institute of Michigan, Ann Arbor, March 1995.

[2] R.G. Paxman, B.J. Thelen, L.S. Joyce, R.L. Sullivan, and M.T. Eismann, *PRISM Detection Modeling*, ERIM Final Report No. 246835-18-F, July 1994.

[3] I. Cindrich, et al., *Passive Interferometric Range Angle Imaging*, ERIM Report No. 179200-110-F to AFWAL, Air Force Report No. WL-TR-1059, December 1991.

[4] B.D. Neagle, and A. Klooster, *Mobile PRISM Demo Image Database*, ERIM Report No. 246840-1-F Vol 2., March 1995.

Table 4. PRISM Data Collection Log

Run #	Date/Time	Site #	Description	Net	Data Type	Sources	Conditions
1	6/20/94 3:14pm	1	HMMWV with canvas & North Heading	Yes	Real Data 61 Positions	Edge 38/25 Line 37/26	Light Wind < ≈5 mph Bright Sun
2	6/20/94 3:32pm	1	HMMWV with canvas & North Heading	Yes	Complex Data 31 Positions	Edge 39/29 Line 36/27	Light Wind < ≈5 mph Bright Sun
3	6/20/94 3:49pm	1	HMMWV with canvas & North Heading	Yes	No Gratings	Edge 40/30 Line 32/25	Light Wind < ≈5 mph Bright Sun
4	6/20/94 4:21pm	1	HMMWV under net	Yes	No Gratings	Edge 40/38 Line 38/25	Light Wind < ≈5 mph Bright Sun
5	6/20/94 4:34pm	1	HMMWV under net	Yes	Real Data	Edge 37/26 Line 35/22	Light Wind < ≈5 mph Bright Sun
6	6/20/94 4:56pm	1	HMMWV under net	Yes	Complex Data	Edge 36/26 Line 36/22	Light Wind < ≈5 mph Bright Sun
7	6/20/94 5:15pm	1	HMMWV in road heading West (All runs 1-7 HMMWV had canvas on back)	Yes	Complex Data	Edge 35/26 Line 35/22	Light Wind < ≈5 mph Bright Sun
8	6/20/94 5:32pm	1	Last position is bad	Yes	Real Data	Edge 34/26 Line 36/22	Light Wind < ≈5 mph Bright Sun
9	6/20/94 5:47pm	1	Last position is bad	Yes	No Gratings	Edge 31/23 Line 35/22	Light Wind < ≈5 mph Bright Sun
10	6/20/94 6:14pm	1	Isuzu under net	Yes	No Gratings		Clouds
11	6/20/94 6:30pm	1	Isuzu under net	Yes	Real Data	Edge 38/22 Line 35/21	Clouds
12	6/20/94 6:53pm	1	HMMWV in trees recently run (hot) Isuzu under net	Yes	Real Data		Clouds

Table 4. PRISM Data Collection Log (Continued)

Run #	Date/Time	Site #	Description	Net	Data Type	Sources	Conditions
13	6/20/94 7:06pm	1	HMMWV in trees recently run (hot) Isuzu under net	Yes	Complex Data	Edge 35/20 Line 32/21	Cloudy No Wind
14	6/20/94 7:23pm	1	HMMWV in trees recently run (hot) Isuzu under net	Yes	No Gratings	Edge 33/20 Line 29/21	Cloudy No Wind
15	6/20/94 7:40pm	1	HMMWV heading NE in open	Yes	No Gratings	Edge 31/20 Line 29/20	Cloudy No Wind
16	6/20/94 7:57pm	1	HMMWV heading NE in open	Yes	Real Data	Edge 30/19 Line 29/20	Cloudy No Wind
17	6/20/94 8:37pm	1	HMMWV heading NE in open	Yes	Completely Dark	Edge 28/19 Line 29/20	Cloudy No Wind
18	6/20/94 8:53pm	1	HMMWV in road	Yes	Real Data	Edge 28/19 Line 25/19	Cloudy No Wind
19	6/20/94 9:10pm	1	HMMWV in road	Yes	No Gratings		Cloudy No Wind
20	6/22/94 12:41pm	1	Truck is near bridge heading SSE (M-35) (Lights in Scene)	No	Real Data	Edge 44/28 Line 33/26	Mostly Sunny (75% sun) Light Wind < ≈5 mph
21	6/22/94 12:59	1	Truck is near bridge heading SSE	No	Real Data	Edge 46/35 Line 33/30	Mostly Sunny (75% sun) Light Wind < ≈5 mph
22	6/22/94 1:21pm	1	Truck is near bridge heading SSE	No	Complex Data	Edge 27/36 Line 41/31	Mostly Sunny (75% sun) Light Wind < ≈5 mph
23	6/22/94 1:39pm	1	Truck heading West	No	Real Data	Edge 46/35 Line 38/25	Mostly Sunny (75% sun) Light Wind < ≈5 mph
24	6/22/94 2:46pm	1	Truck heading West	No	Real Data	Edge 45/30 Line 34/24	Mostly Sunny (75% sun) Light Wind < ≈5 mph
25	6/22/94 3:04pm	1	Truck heading West	No	No Gratings	Edge 44/28 Line 37/25	Mostly Sunny (75% sun) Light Wind < ≈5 mph

Table 4. PRISM Data Collection Log (Continued)

Run #	Date/Time	Site #	Description	Net	Data Type	Sources	Conditions
26	6/22/94 6:46pm	1	M-35 in trees this run was overwritten	No	No Gratings		Mostly Sunny (75% sun) Light Wind < ≈5 mph
27	6/22/94 3:38pm	1	M-35 in trees	No	Real Data	Edge 42/28 Line 40/24	Sunny Light Wind < ≈5 mph
28	6/22/94 3:59pm	1	M-35 in trees	No	Complex Data	Edge 40/28 Line 35/20	Sunny Light Wind < ≈5 mph
29	6/22/94 4:28pm	1	M-35 in road last point may have motion	No	Real Data	Edge 37/24 Line 38/18	Sunny Light Wind < ≈5 mph
30	6/22/94 4:44pm	1	M-35 in road last point may have motion	No	Real Data	Edge 37/26 Line 30/19	Sunny Light Wind < ≈5 mph
31	6/22/94 5:00pm	1	M-35 in center heading East	No	No Grating		Sunny Light Wind < ≈5 mph
32	6/22/94 5:21pm	1	M-35 in center heading East	No	No Grating	Edge 33/21 Line 30/17	Sunny Light Wind < ≈5 mph
33	6/22/94 5:36pm	1	M-35 in center heading East	No	Real Data	Edge 28/17 Line 3/15	Sunny Light Wind < ≈5 mph
34	6/22/94 7:17pm	1	M-35 in center heading East	No	Real Data	Edge 26/16 Line 22/14	Sunny Light Wind < ≈5 mph
35	6/22/94 7:37pm	1	M-35 in center heading North; Canvas up	No	Real Data	Edge 25/14 Line 22/13	Sunny Light Wind < ≈5 mph
36	6/22/94 7:53pm	1	M-35 in center heading North; Canvas up	No	No Gratings		No Wind Mostly Clear
37	6/22/94 8:23pm	1	Truck fronts on road heading NW	No	No Gratings Real Data	Edge 25/10 Line 20/11	No Wind Mostly Clear
38	6/22/94 8:40pm	1	Truck fronts on road heading NW	No	Real Data	Edge 23.3/10 Line 22/11	No Wind Mostly Clear
39	6/22/94 9:17pm	1	Truck in road heading West	No	Real Data	Edge 20/10 Line 20/10	No Wind Mostly Clear

Table 4. PRISM Data Collection Log (Continued)

Run #	Date/Time	Site #	Description	Net	Data Type	Sources	Conditions
40	6/22/94 9:28pm	1	Truck in road heading West	No	No Gratings		No Wind Mostly Clear
41	6/23/94 1:04pm	2	Site #2 HMMWV in center heading West	Yes	Real Data	Edge 41/32 41/30 Line 35/28	Hazy Sun Light Wind <= 5 mph
42	6/23/94 1:28pm	2	HMMWV in center heading West	Yes	Real Data	Edge 43/30 Line 35/28	Hazy Sun Light Wind <= 5 mph
43	6/23/94 1:58pm	2	HMMWV under net	Yes	Real Data	Edge 41/24 39/29 Line 37/20	Hazy Sun Light Wind <= 5 mph
44	6/23/94 2:09pm	2	HMMWV under net	Yes	No Gratings		Mostly Cloudy
45	6/23/94 2:40pm	2	HMMWV under net	Yes	Real Data	Edge 36/30 Line 40/30	Mostly Cloudy
46	6/23/94 3:09pm	2	HMMWV in center heading WSW	Yes	Real Data	Edge 38/28 Line 33/24	Mostly Cloudy
48	6/23/94 3:44pm	2	HMMWV in center heading WSW	Yes	No Gratings		Mostly Cloudy
49	6/23/94 4:25pm	2	HMMWV with back in trees	Yes	No Gratings		Mostly Cloudy
50	6/23/94 4:38pm	2	HMMWV with back in trees	Yes	Complex Data	Edge 34/24 Line 32/22	Mostly Cloudy
51	6/23/94 4:54pm	2	HMMWV with back in trees	Yes	Real Data	Edge 34/24 Line 32/22	Mostly Cloudy
52	6/23/94 5:08pm	2	HMMWV in road	Yes	Real Data	Edge 33/23 Line 32/22	Mostly Cloudy
53	6/23/94 5:22pm	2	Kid walked through	Yes	Complex Data	Edge 33/23 Line 32/22	Mostly Cloudy
54	6/23/94 5:39pm	2	Kid walked through	Yes	No Gratings		Mostly Cloudy

Table 4. PRISM Data Collection Log (Continued)

Run #	Date/Time	Site #	Description	Net	Data Type	Sources	Conditions
55	7/26/94 3:01pm	1	HMMWV heading South Time still set 1 hour early	No	Real Data	Line 31/20	Mostly Sunny Very windy ≈10-20 mph on bridge.
56	7/26/94 4:26pm	1	HMMWV heading South	No	Real Data	Line 34/24	Partly Sunny
57	7/26/94 4:49pm	1	HMMWV heading South	No	Real Data	Line 35/24	Partly Sunny
58	7/26/94 5:13pm	1	HMMWV nose at tree line	No	Real Data	Line 35/26	Moderate Wind 10-20 on bridge; 5-10 on ground
59	7/26/94 5:37pm	1	HMMWV nose at tree line	No	Real Data	Line 34/22	Moderate Wind 10-20 on bridge; 5-10 on ground
60	7/26/94 5:59pm	1	HMMWV nose at tree line	No	Real Data	Line 35/18	Moderate Wind 10-20 on bridge; 5-10 on ground
61	7/26/94 6:35pm	1	HMMWV heading North Camo-net wetted in areas	Draped	Real Data	Line 30/21	Light Wind 0-5 mph
62	7/26/94 6:55pm	1	HMMWV heading North Camo-net wetted in areas	Draped	Real Data	Line 30/20	Light Wind
63	7/26/94 7:20pm	1	Truck ahead ≈8 ft	Draped	Real Data	Line 30/19	No Wind Mostly Clear
64	7/26/94 7:45pm	1	Truck ahead ≈8 ft	Draped	Real Data	Line 29/19	No Wind Mostly Clear
65	7/26/94 8:34pm	1	Truck ahead ≈8 ft heading NNE	Draped	Real Data	Line 29/15	No Wind Mostly Clear
66	7/26/94 8:57pm	1	Truck ahead ≈8 ft heading NNE	Draped	Real Data	Line 18/13	No Wind Mostly Clear
67	7/26/94 9:24pm	1	Truck ahead ≈8 ft heading NNE	Draped	Real Data	Line 18/13	No Wind Mostly Clear
68	9/26/94 10:04pm	1	Truck ahead ≈8 ft heading NNE	Draped	Real Data	Line 18/14	No Wind Mostly Clear

Table 4. PRISM Data Collection Log (Continued)

Run #	Date/Time	Site #	Description	Net	Data Type	Sources	Conditions
69	7/26/94 10:30pm	1	HMMWV moved forward ≈10 ft; Heading NE	Draped	Real Data	Line 18/13	No Wind Mostly Clear
70	7/26/94 10:52pm	1	HMMWV Headed NE	Draped	Real Data		
72	7/27/94 2:43pm	2	HMMWV Heading West	No	Real Data		
73	7/27/94 3:13pm	2	HMMWV in center heading West	No	Real Data	Line 32/22	Overcast, Very Light Wind <5 mph
74	7/27/94 3:33pm	2	HMMWV in center heading West	No	Real Data	Line 31/22	Overcast, Very Light Wind <5 mph
75	7/27/94 3:52pm	2	HMMWV on road heading NE	No	Real Data	Line 31/21	Overcast, Very Light Wind <5 mph
76	7/27/94 4:14pm	2	HMMWV on road back under trees	No	Real Data		Spitting Rain, Light Wind <5 mph
77	7/27/94 4:32pm	2	HMMWV on road back under trees	No	Real Data	Line 31/21	Spitting Rain
78	7/27/94 4:53pm	2	HMMWV on road back under trees; Water put on hood	No	Real Data	Line 30/23	Spitting Rain
79	7/27/94 5:29pm	2	HMMWV moved ahead 10 ft	No	Real Data	Line 30/20	Spitting Rain
80	7/27/94 5:51pm	2	Water on hood and canvas to reduce contrast	No	Real Data		Spitting Rain
81	7/27/94 6:14pm	2	HMMWV moved ahead 10 ft	No	Real Date	Line 30/20	Spitting Rain
82	7/27/94 6:38pm	2	HMMWV heading SW	No	Real Data		Spitting Rain
83	7/27/94 7:22pm	2	HMMWV heading SW	No	Real Data	Line 29/16	Spitting Rain

Table 4. PRISM Data Collection Log (Continued)

Run #	Date/Time	Site #	Description	Net	Data Type	Sources	Conditions
84	7/27/94 7:55pm	2	HMMWV heading SW	No	Real Data	Line 29/16	Spitting Rain
85	7/27/94 8:16pm	2	HMMWV on road heading ESE	No	Real Data	Line 29/16	Spitting Rain

APPENDIX A

Field Site Survey Procedures

A physical survey of the target area was performed for each of the three test sites at Kinzua Bridge. A 30 second digital readout theodolite with EDM (electronic distance measurement) was used to survey sensor and target locations. The complete survey consisted locating the following:

Midpoint of sensor travel
Primary and secondary retroreflectors
Calibration targets and test vehicles
Natural terrain features

The following procedure was used for surveying the three sites. A diagram of the aim point geometry is shown in Figure 14.

1. Choose the location for the primary aim point P and drive a survey stake to mark the location (position 1).

2. Set up the theodolite over the primary stake, measure and record the range and vertical angle to a retroreflector held at the estimated midpoint of the sensor travel (position 2).

3. At the bridge, move approximately 300 feet along the track, set up the retroreflector and mark the bridge railing. From the ground, measure and record the range to the retroreflector using the theodolite and EDM (position 3).

4. Compute the distance from the mark on the rail to the center of travel by using the following formula:

$$BC = \sqrt{(PC^2 - PB^2)}$$

Where PC - Distance from position 1 to position 2

PB = Distance from position 1 to position 3

BC = Distance from position 3 to exact center

5. Measure back the distance BC computed above to the location of the exact center of sensor travel and mark the bridge rail.

6. Compute the required distance between primary and secondary retroreflectors using the following formula:

   $PS = PC^* 2.5/16$

7. Stretch a light weight nylon line horizontally from the primary retroreflector location extending past the approximate location of the secondary retroreflector.

8. Move the free end of the line laterally to bring it parallel to the bridge railing by observing the line and the railing visually from below. Insure that the line is also horizontal by using a line level at the middle of the line. Stake and tie the free end of the line when proper alignment is achieved.

9. Measure the primary to secondary distance along the line and mark the approximate location of the secondary with a survey stake.

10. Compute the height of the secondary retroreflector above the line:

    $H = PC^* (2.5/16)^2$

11. Position the secondary retroreflector on a suitable pole at the required distance form P and height above the line H. Relocated if necessary to position the retroreflector on visual line between the bridge railing and the line secured in step 8. Align the retro axis roughly with point C. Use guy lines to secure the pole and retroreflector in this location.

12. Mount the primary retroreflector securely at point P with its axis aligned to point C.

Following the location of the primary and secondary retroreflectors, the theodolite and EDM were used to measure the polar coordinates to specified points on any test targets and vehicles located in the scene. The locations of natural terrain features such as vehicle tracks, bushes, and large rocks was also noted and recorded.

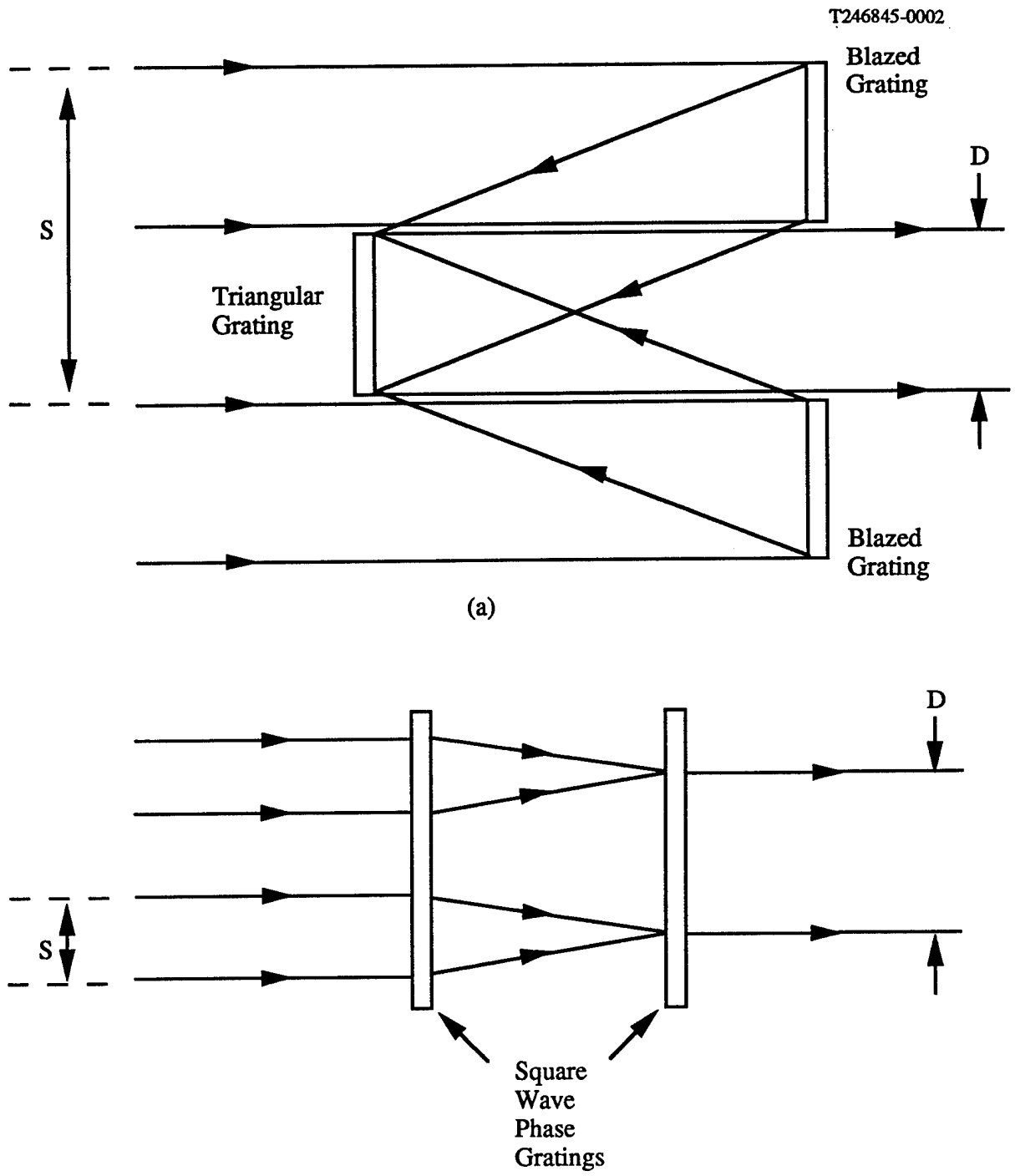

Figure 1. Grating Interferometer (a) Reflective (b) Transmissive

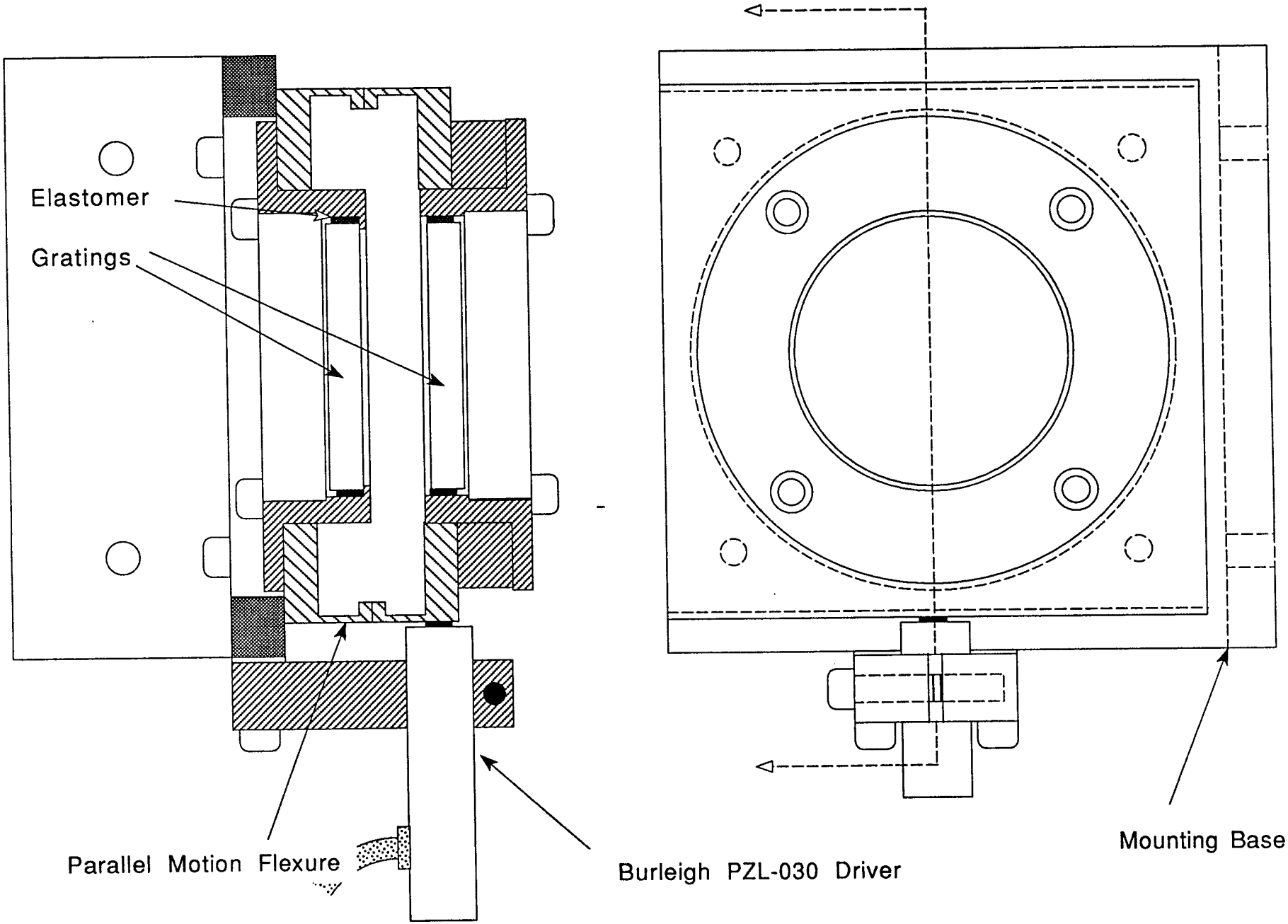

Figure 2. Grating Mount

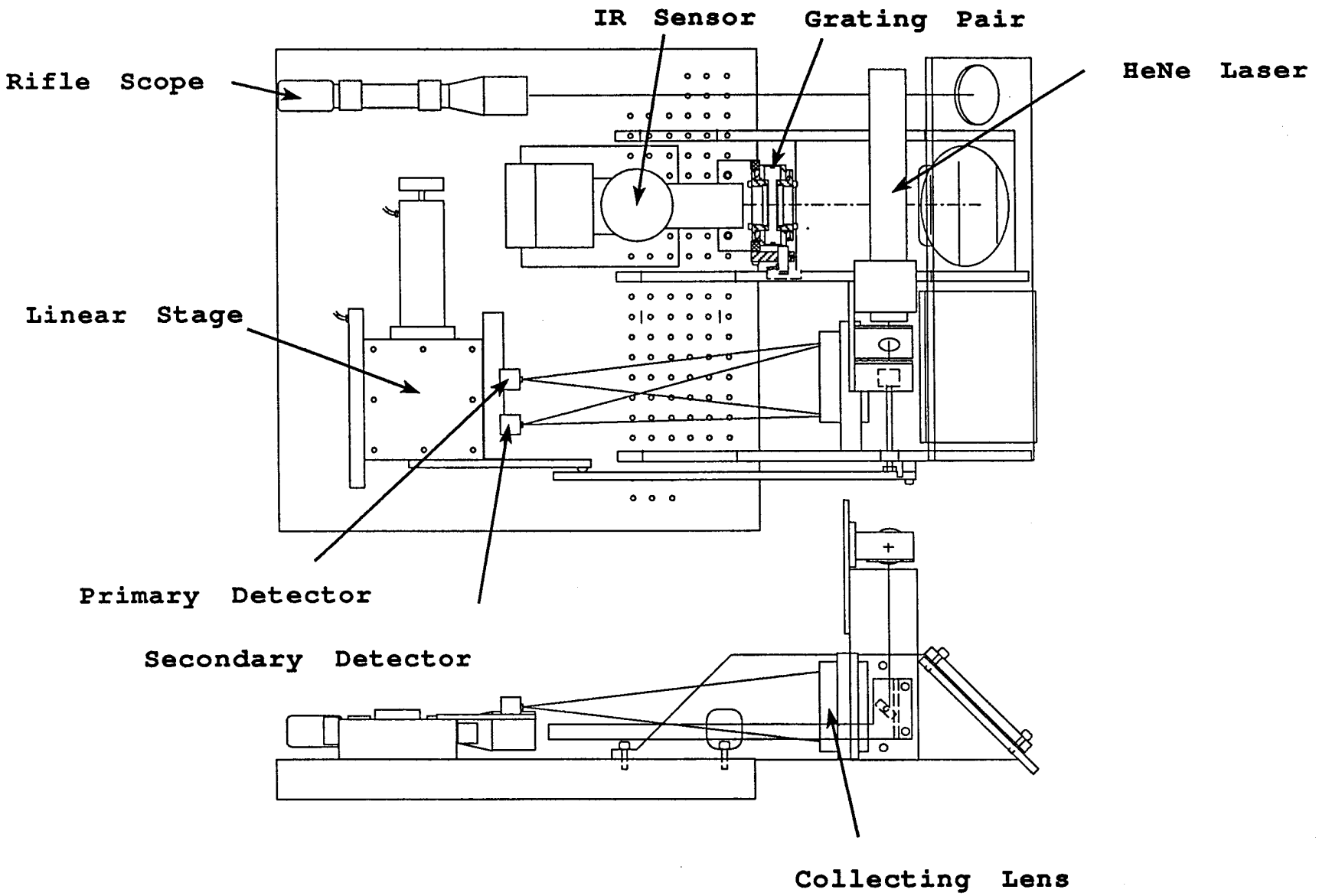

Figure 3. PRISM Sensor Layout

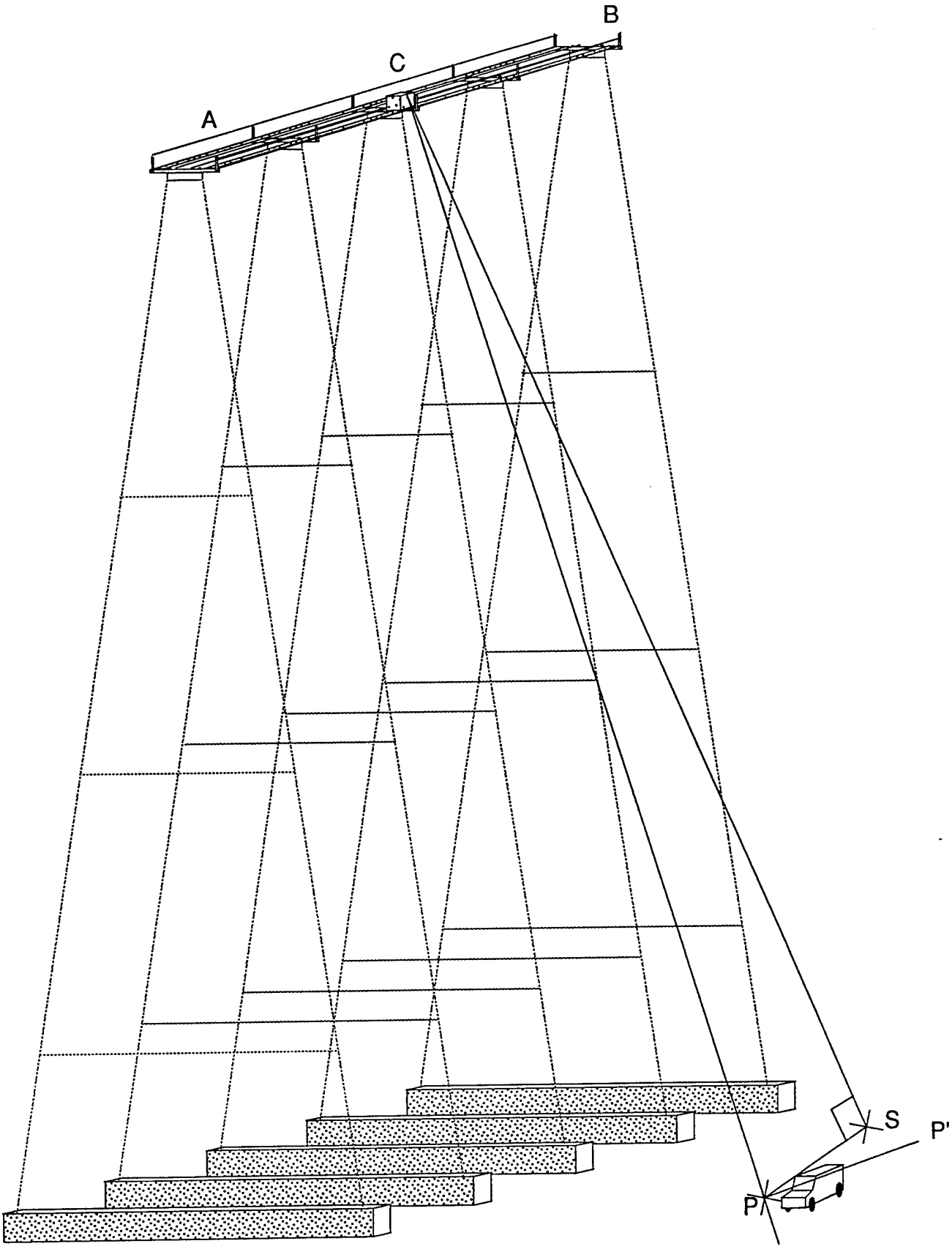

Figure 4. PRISM Data Collection Geometry

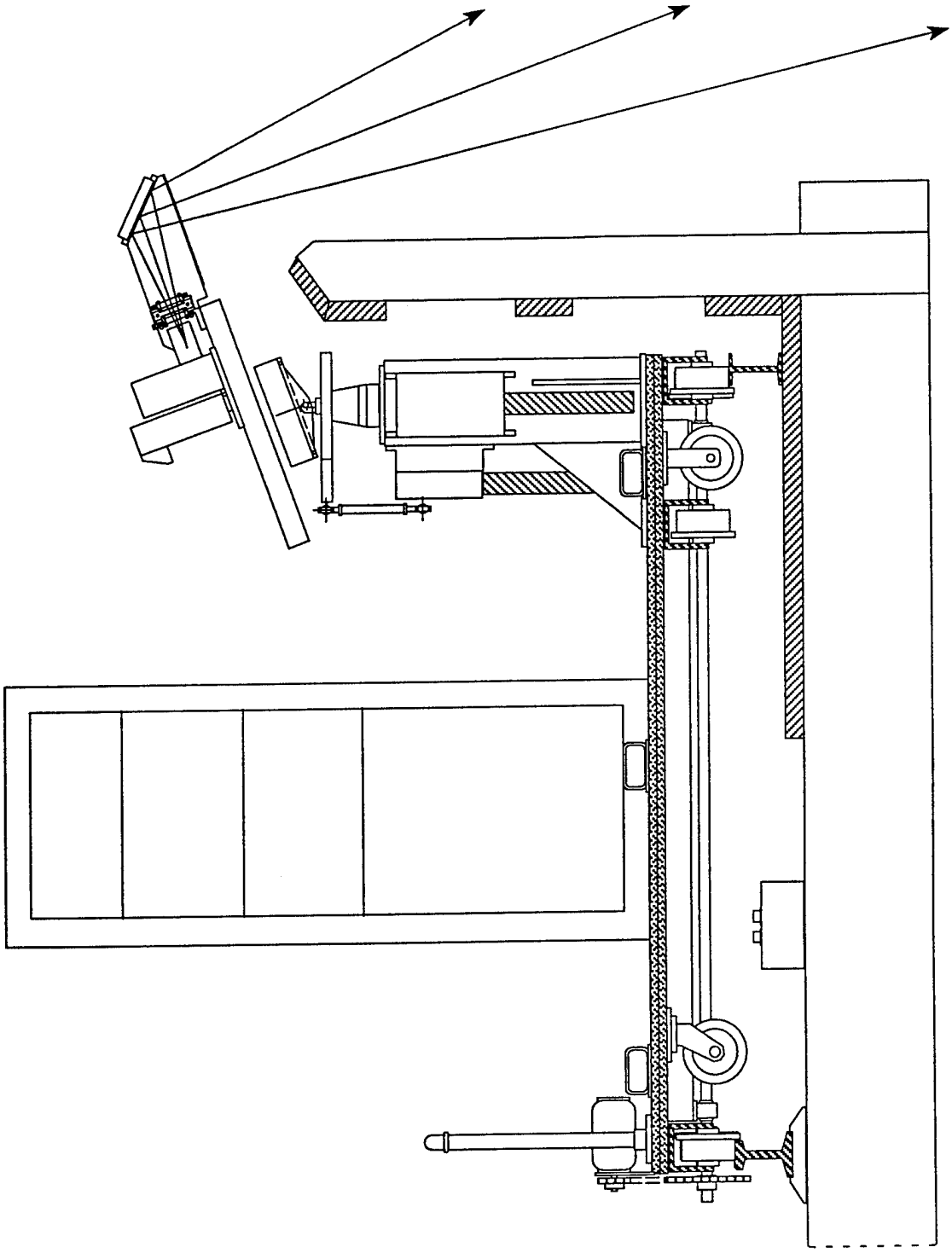

Figure 5. PRISM Sensor Vehicle

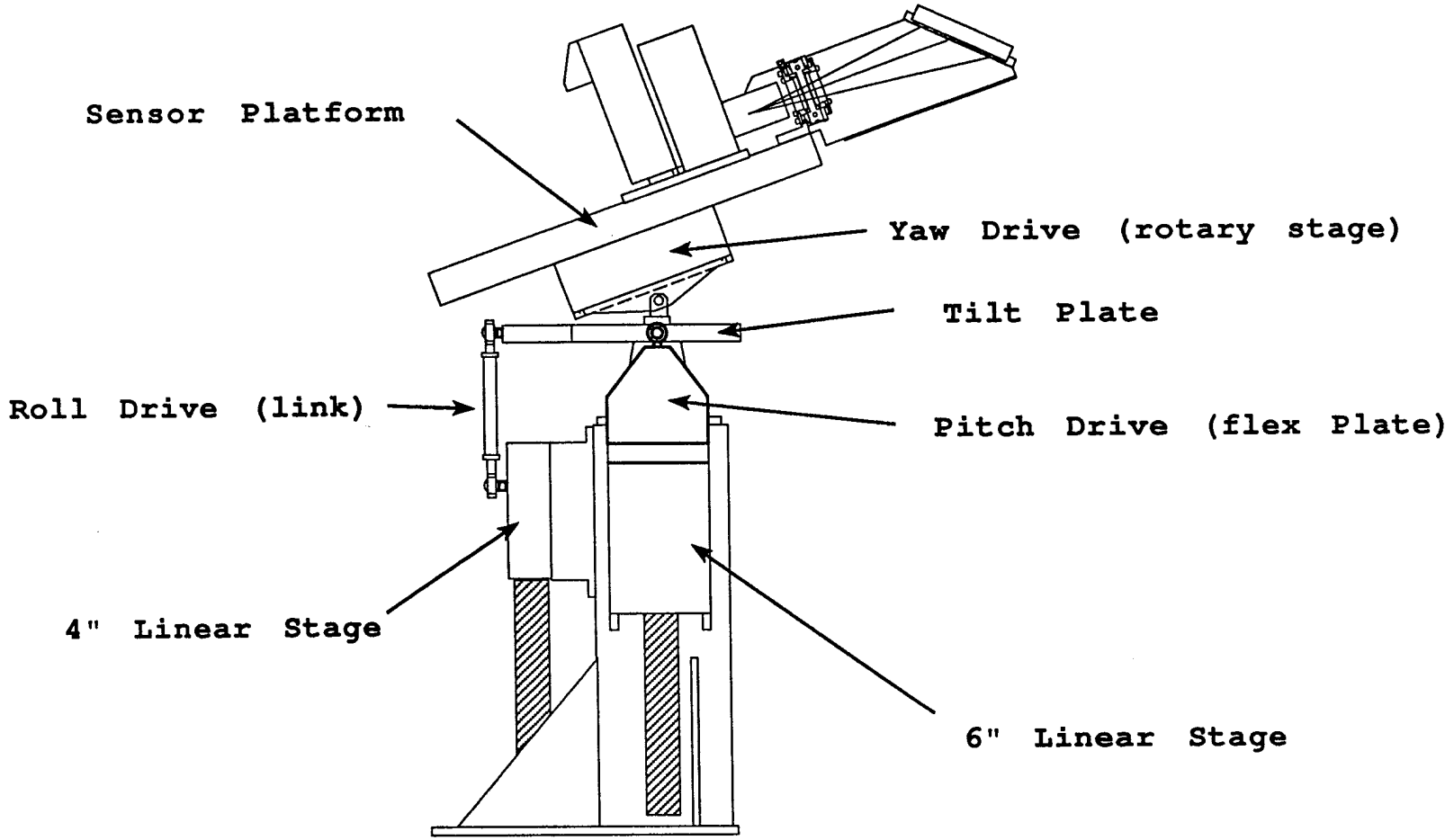

Figure 6. PRISM Pedestal

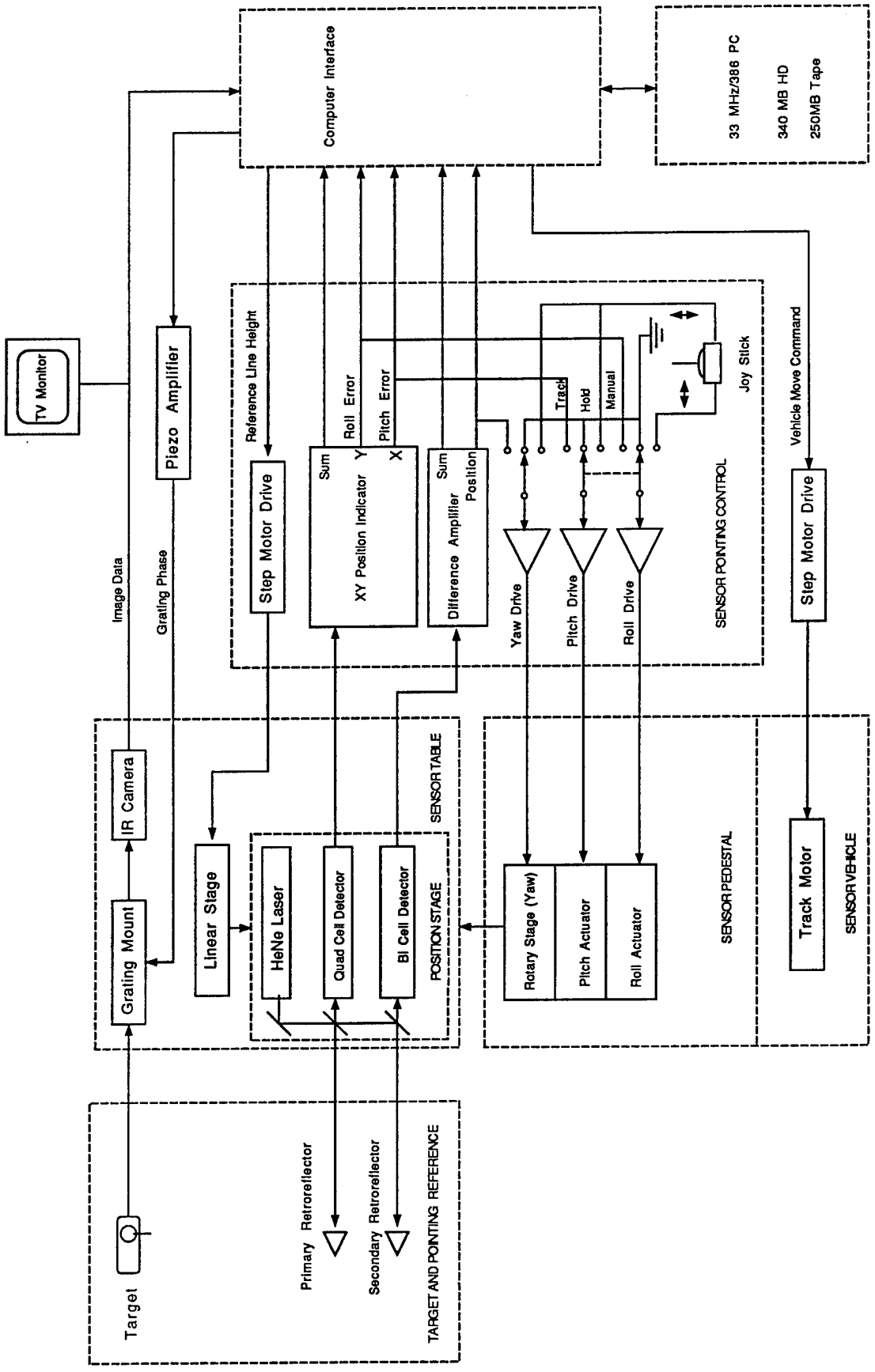

Figure 7. PRISM Sensor System Block Diagram

Mobile PRISM Control Program Flow

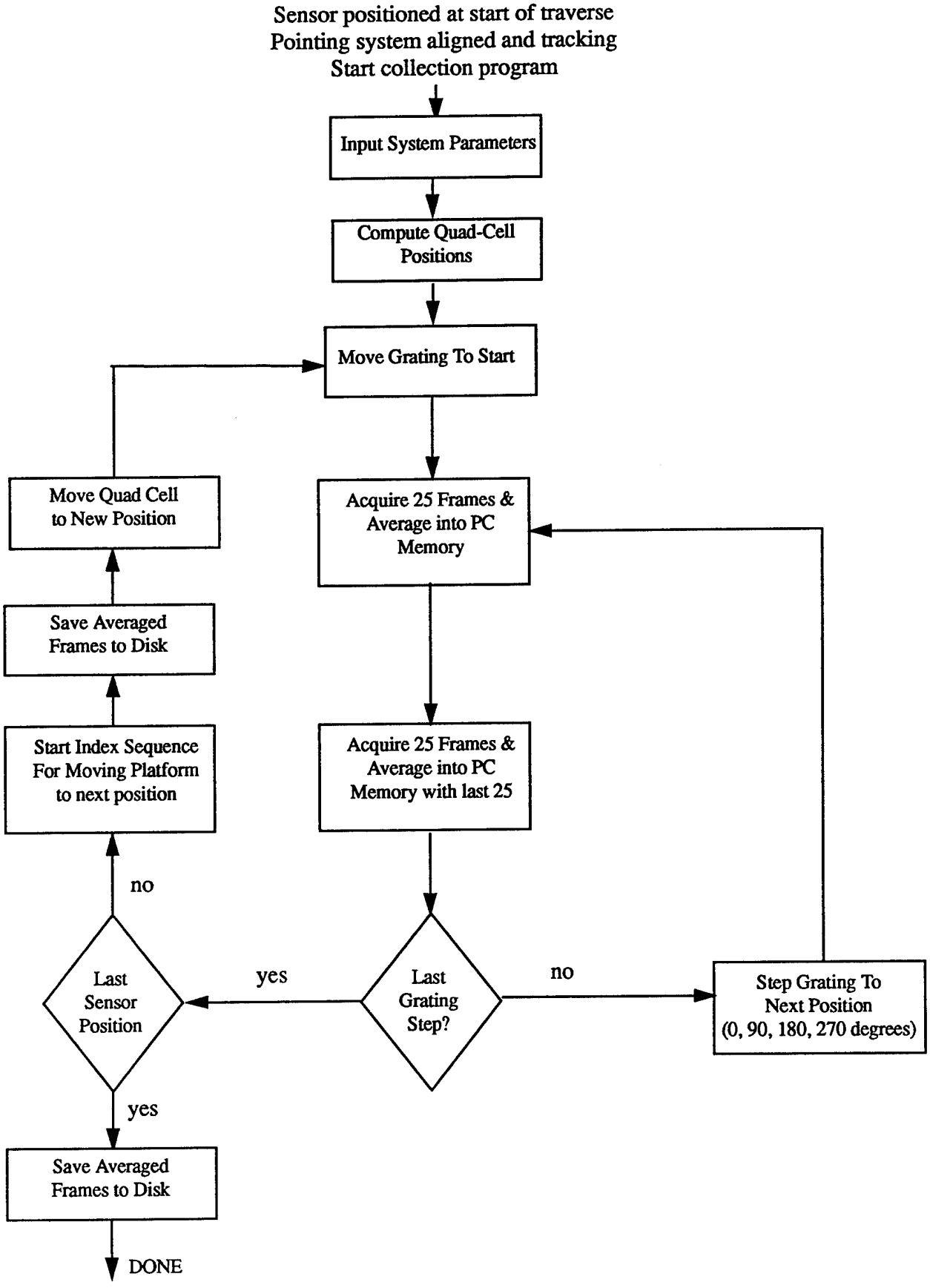

Figure 8. PRISM Control Program Flow Chart

Mobile PRISM Improved Control Program Flow

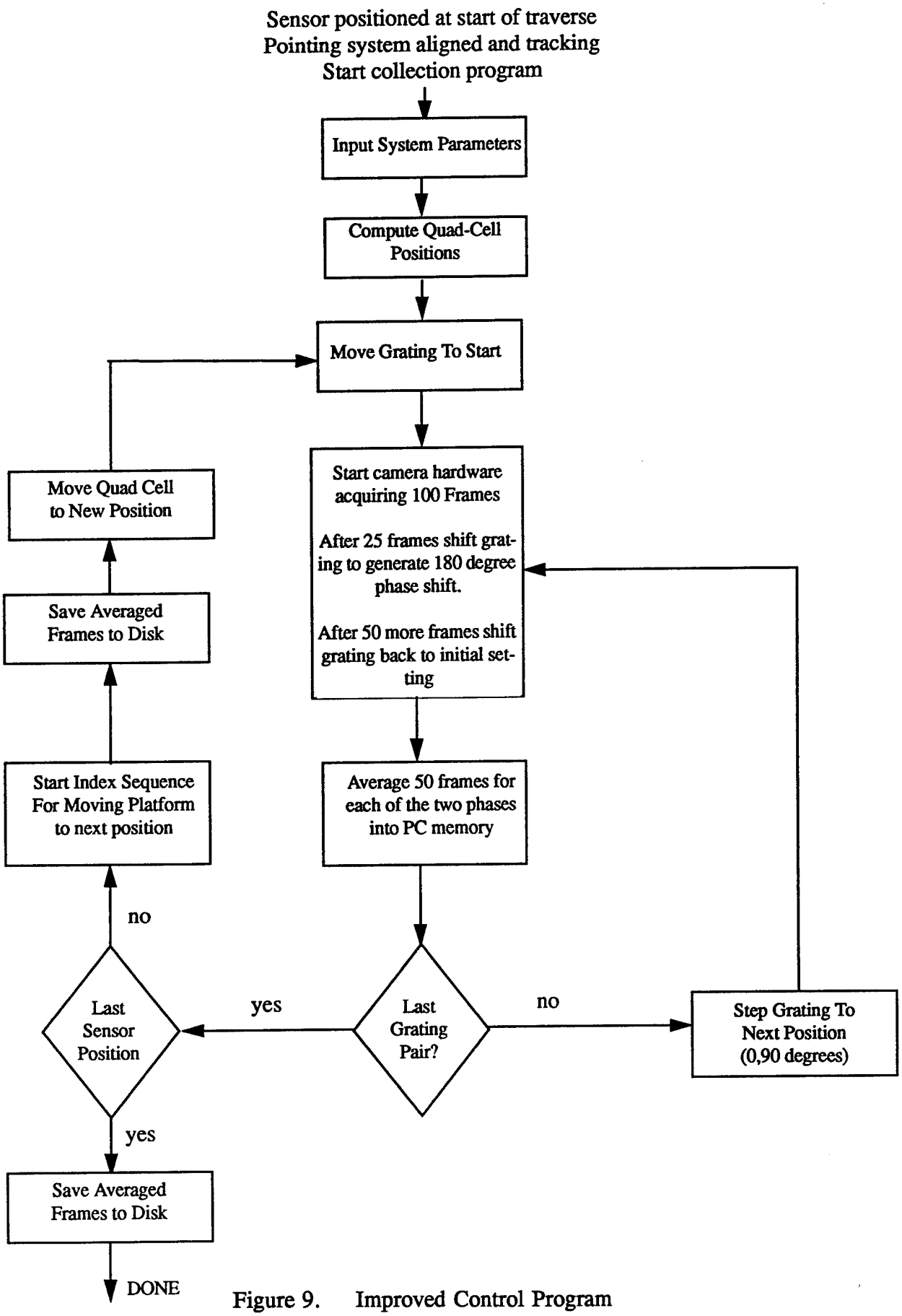

Figure 9. Improved Control Program

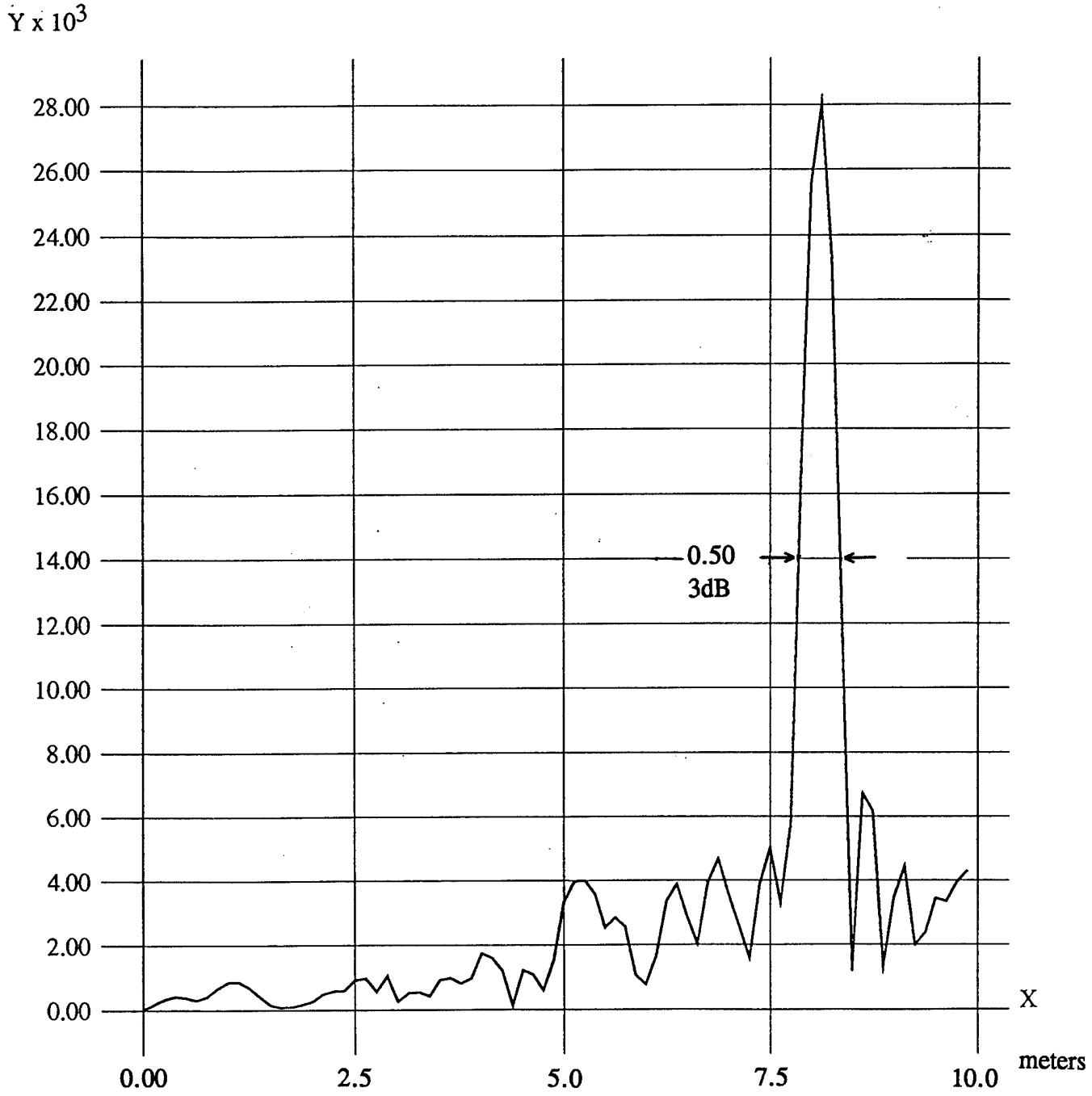

Figure 10. PRISM System Impulse Response

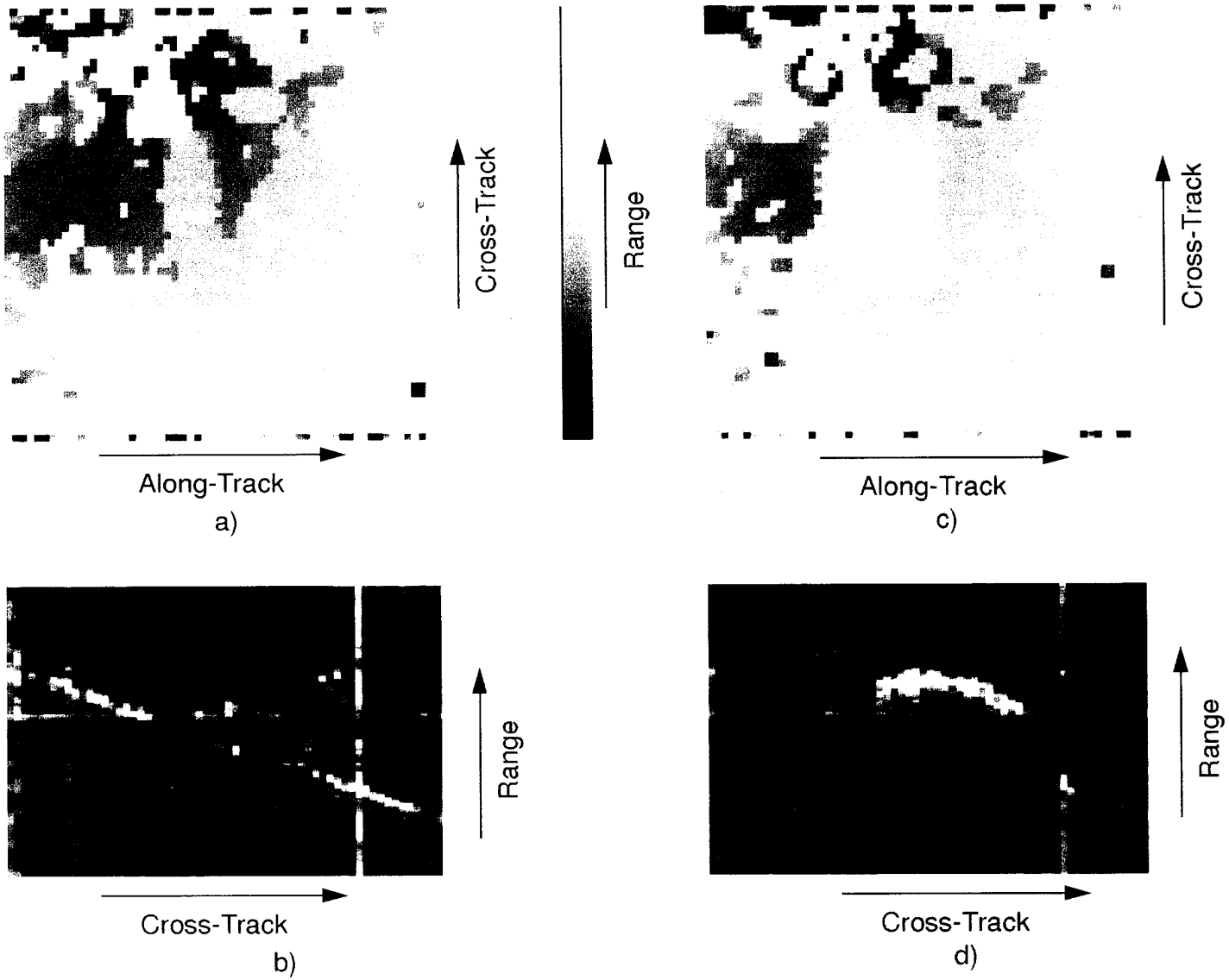

Figure 11. Sensor 3-D Image Results for Open and Netted M35 Trucks: (a) and (c) Grey Scale Encoded Range Maps, and (b) and (d) Limited Projected in the Along Track Ground Plane Direction

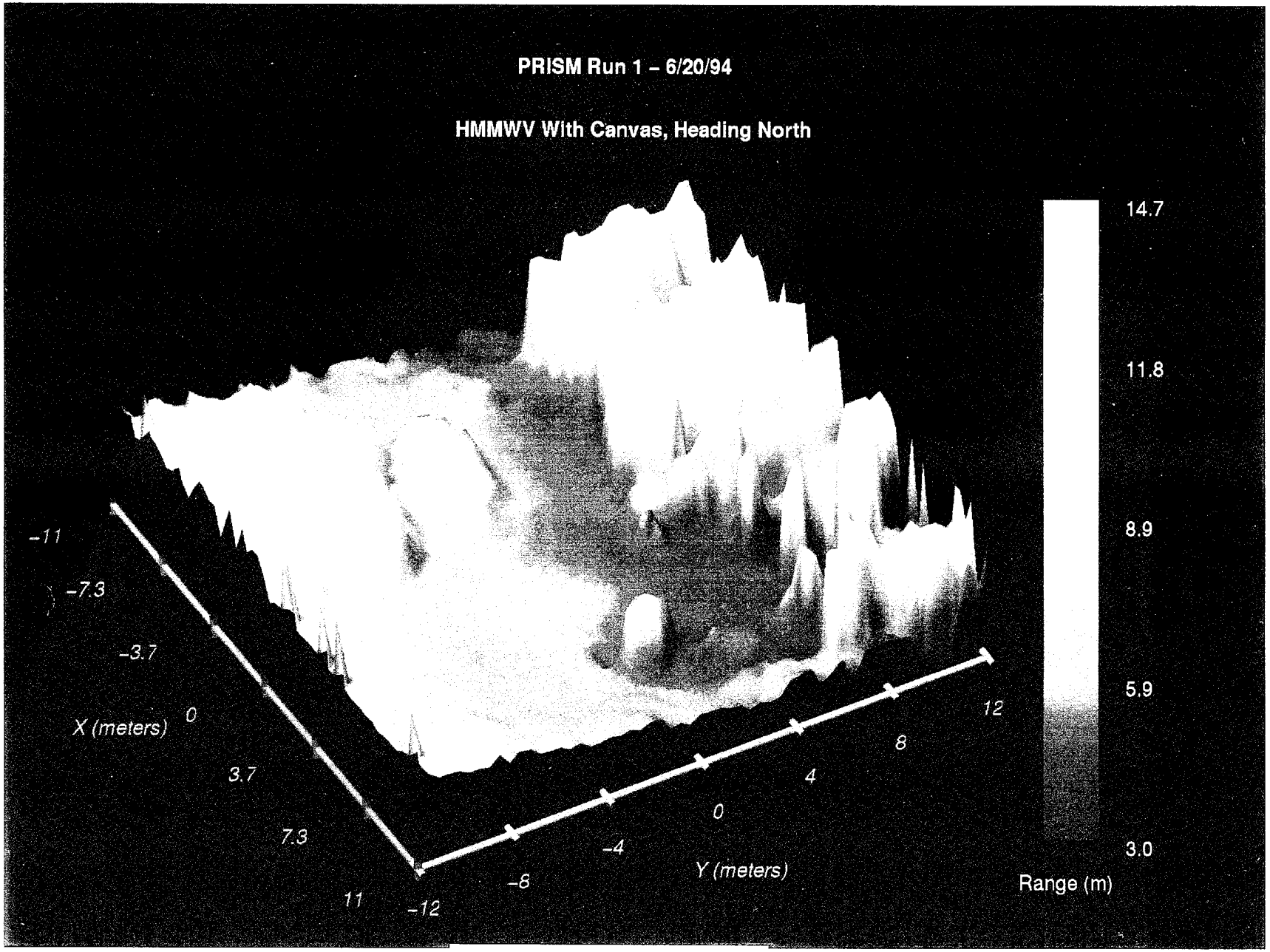

Figure 12. 3-D Surface Plot

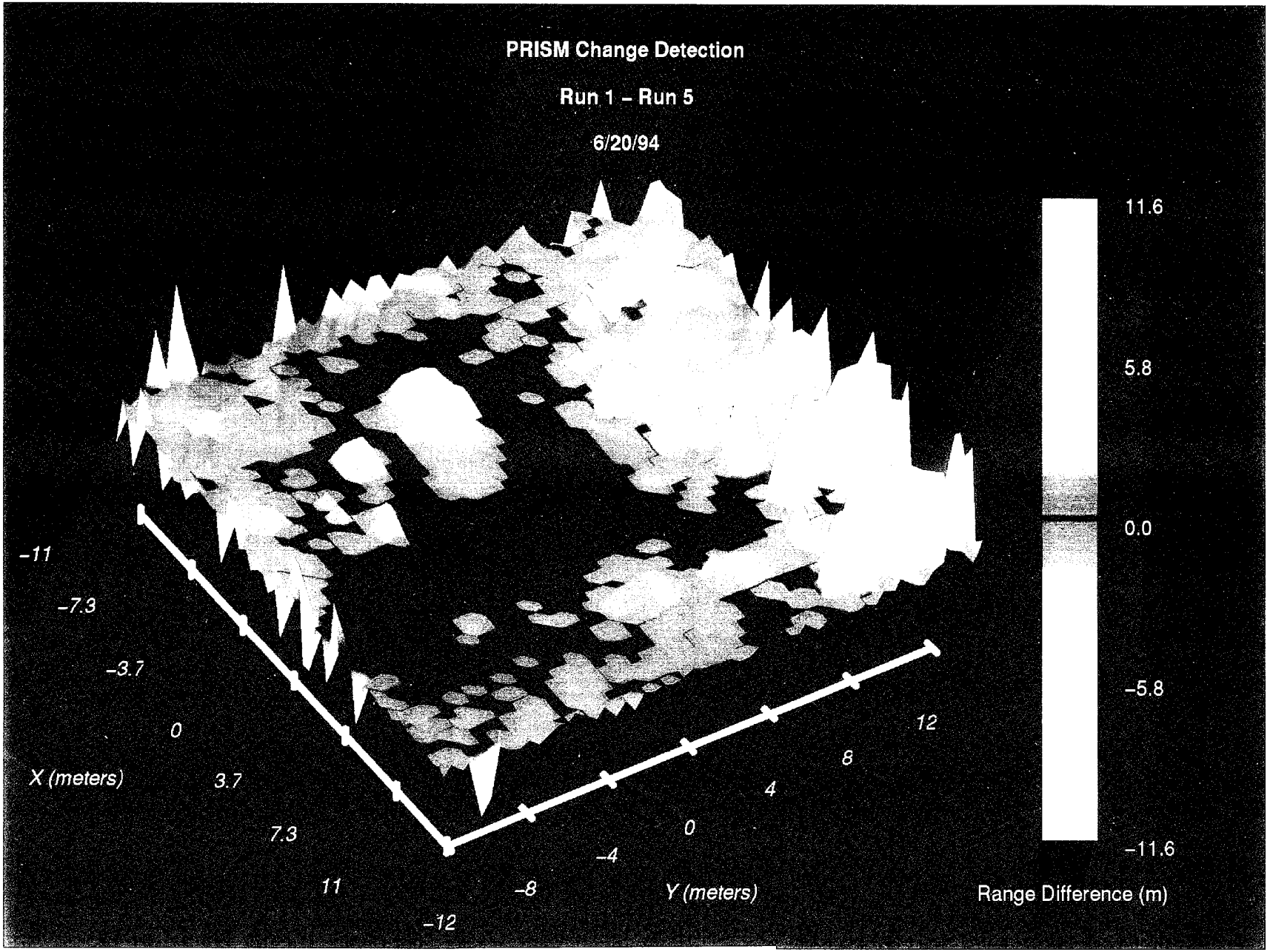

Figure 13. Change Detection

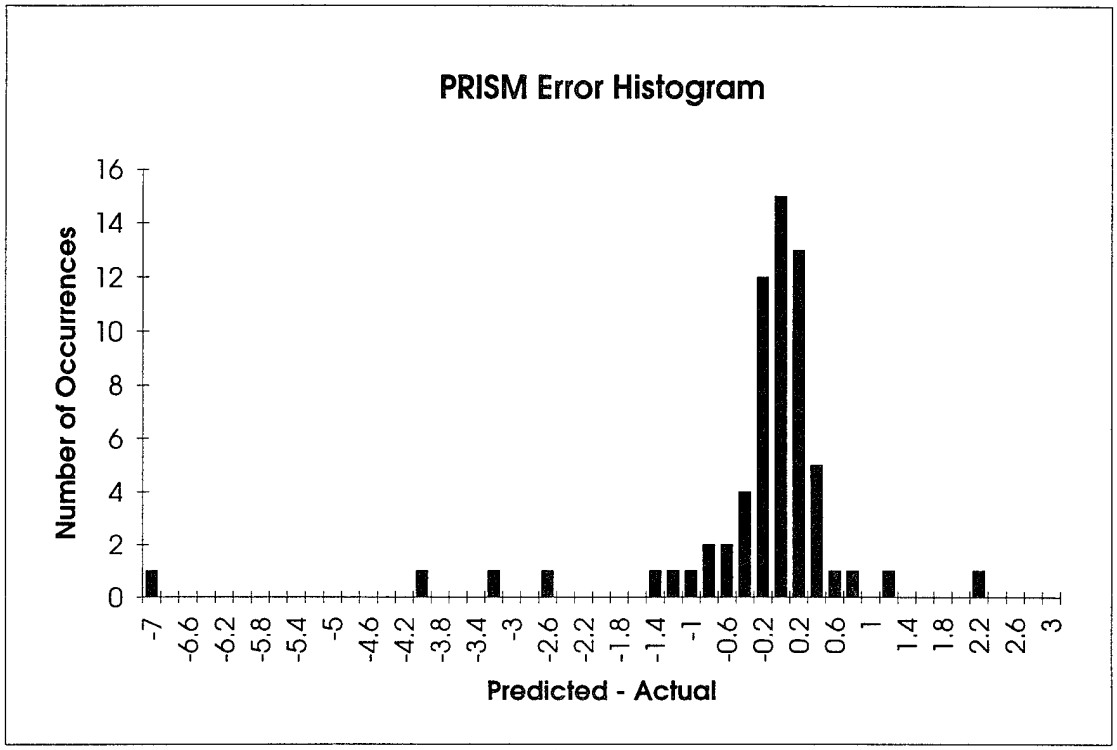

(a)

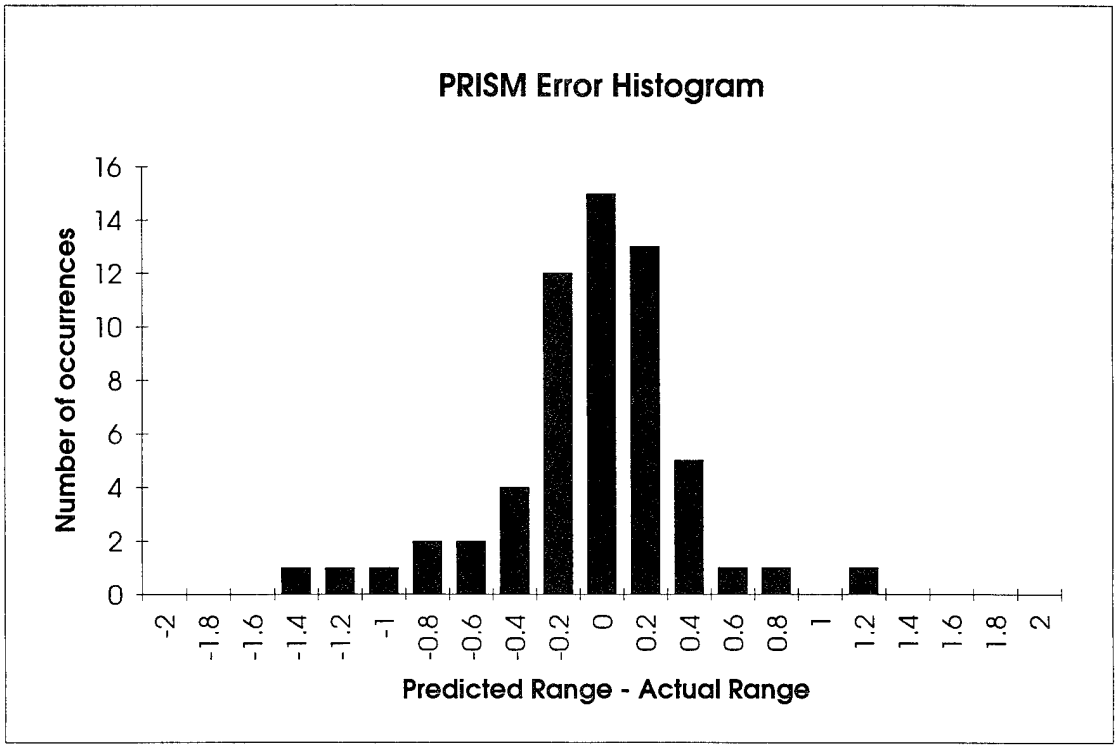

(b)

Figure 14. Ranging Error Distribution (a) All Measured Points (b) ± 2 Meter Limit